INTERNATIONAL JOURNAL FOR NUMERICAL AND ANALYTICAL METHODS IN GEOMECHANICS, VOL. 20, 517–544 (1996)

LOAD DISTRIBUTION ALONG FULLY GROUTED BOLTS, WITH EMPHASIS ON CABLE BOLT REINFORCEMENT

A. J. HYETT, M. MOOSAVI AND W. F. BAWDEN

Department of Mining Engineering, Queen's University, Kingston, Ontario, Canada

SUMMARY

Explanation for the widely reported observation that fully grouted reinforcement is more effective in hard rock that behaves as a discontinuum than in soft rock is presented. Analytical solutions are presented for the distribution of displacement and load along an untensioned fully grouted elastic bolt, of specified bond stiffness, which is activated during excavation by either a continuous or discontinuous distribution of rock displacement. The results indicate that significantly higher axial loads are developed for the discontinuous case.

Since the mechanics of bond failure depend on the type of bolt and grout used, in the second part of the paper a finite difference formulation is introduced and combined with a non-linear model for the bond behaviour of a cement grouted seven-wire strand cable bolt. The results of a parametric study indicate that, because the bond is frictional and depends on confinement at the borehole wall, for the same profile of rock mass displacement lower loads are developed in soft rock. Furthermore, in soft rock, excavation induced stress changes can cause a dramatic reduction in bond strength, so that, even after significant rock mass displacement, the axial load developed is significantly less than the tensile strength of the cable. A combination of these effects can explain why failures of cable bolted ground involve debonding at the cable–grout interface in soft rock, and why instances of cable rupture are confined to hard, blocky rock masses.

KEY WORDS: rock reinforcement; load distribution; cable bolts; fully grouted

INTRODUCTION

Hoek and Brown[1] point out that the 'principal objective in the design of underground excavation support is to help the rock mass support itself'. They suggest that 'pre-placed grouted reinforcing elements are probably the most effective means of achieving this objective', and that 'the future will see a great increase in the use of this support technique'. Perhaps in response to such predictions, several papers presented at the International Symposium on Rock Bolting, three years later in 1983, contained detailed information on the distribution of axial loads along untensioned fully grouted rock bolts. In particular, Bjornfot and Stephansson,[2] based on a comparison of their own *in situ* instrumentation results in hard rock and Freeman's[3] results in soft rock, concluded that the behaviour of fully grouted rock bolts depends on the rock mass characteristics.

Another part of these proceedings was devoted to what was then, the relatively recent innovation of *cable bolting*. In his keynote lecture, Fuller[4] discussed the use of fully grouted cables for the *pre-reinforcement* of open stopes in Australia. He also described instances where cable bolting was unsuccessful due to debonding at the cable grout interface. In recent years the increased popularity of cable bolts for both mining and civil applications, is perhaps the most widespread geotechnical application of pre-placed fully grouted reinforcement. Although in

CCC 0363–9061/96/070517–28

Received 6 January 1995
Revised 26 October 1995

general successful, expensive failures of cable bolted ground still occur in many mines. Today, the principal factor inhibiting more cost-effective design remains the limited understanding of how fully grouted reinforcement behaves *in situ*. In particular, why are failures of cable bolted ground due to debonding at the cable–grout interface prevalent in soft rock, and why are the few instances of cable rupture confined to hard, blocky rock masses?

This paper employs both analytical and numerical methods to predict the behaviour of fully grouted bolts for a prescribed distribution of rock mass displacement. Although no attempt is made to simulate rock mass reinforcement interaction in this paper, the numerical formulation is suitable for implementation in numerical stress analysis packages with the capability to do so. The solutions presented provide an opportunity to verify or assess the performance of this and other implementations. Hence, this paper reperesents an interim step in providing engineers with technology to understand the behaviour of, and thus to optimise the design of, bolt length, bolt spacing and bolt pattern of fully grouted reinforcement.

ANALYTICAL TREATMENT

Analysis of ground anchors

In a one-dimensional theoretical analysis of resin grouted anchors, Farmer[5] assumed a circular elastic anchor of radius r with Young's modulus E_b, surrounded by an elastic grount annulus with shear modulus G_g, all confined by a rigid borehole of radius R. He derived a homogeneous linear differential equation describing the distribution of axial displacement (U_x) along the anchor:

$$\frac{d^2U_x}{dx^2} - \alpha^2 U_x = 0 \tag{1}$$

Farmer compared the analytical results based on the solution to (1) with data from instrumented anchors grouted into concrete, limestone and chalk. He found that, whilst at lower anchor loads in the concrete, the measured stress distribution was similar to that predicted theoretically, in the weaker limestone and chalk, significant discrepancies were observed, which he attributed to debonding at the anchor–grout interface.

A more realistic analytical treatment of the same problem was presented by Aydan *et al.*[6] Although still assuming that the bolt was elastic, an idealized elastic-softening plastic behaviour was adopted for the anchor–grout interface, similar to that proposed by St. John and Van Dillen[7] in their numerical representation of fully grouted rock bolts. Solving equation (1) for those lengths of anchor undergoing elastic, softening and residual (perfectly plastic) behaviour, and modifying α to account for elastic shear of the borehole wall, the distribution of displacement and axial load in the bolt were calculated. The results, which simulated progressive debonding of the bolt–grout interface, agreed well with the finite element results obtained by Hollingshead.[8] In a further development, and again following St. John and Van Dillen, Aydan[9] relaxed the assumption of an elastic bolt by assuming a bi-linear elasto-plastic behaviour.

Both of the analyses described solve equation (1) under boundary conditions which are applicable to ground anchors, or pre-tensioned rock bolts. Namely, a tensile force is applied to the bolt or anchor at one end, and in response, according to the assumptions made, deformations are induced in the bolt, and the bolt–grout interface, within the grout annulus and within the rock. However, for fully grouted, untensioned bolts which often have both ends free, the bolt is activated, instead, by rock mass deformations occurring after its installation into the periphery of the excavation (Figure 1).

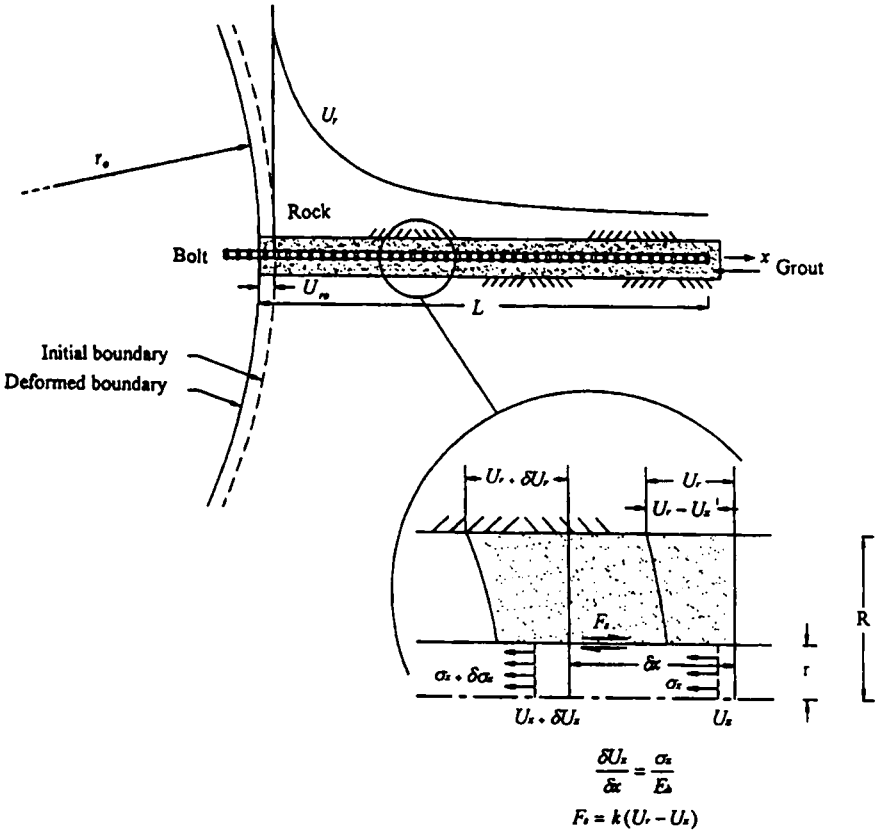

Figure 1. Stress distribution along a fully grouted bolt

Analysis of a fully grouted rigid rock bolt

For a fully grouted bolt, with both ends free, several workers[3,10,11] have realized from equilibrium considerations that the bolt can be divided into two sections. Along the *pick-up length*, positive shear stresses restrain the rock from displacing into the opening, while along the *anchor length* negative shear stresses ensure equilibrium of the bolt. The change in sense of the shear stress occurs at the *neutral point* and coincides with a point of no relative displacement between the rock and the bolt, and also a maximum in the axial tensile load. This effect is clearly evident in the *in situ* observations presented by Xueyi.[12]

Yu and Xian[10] considered a grouted bolt with linear shear behaviour at the bolt–grout interface

$$\tau_x = k(U_r - U_x) \tag{2}$$

grouted into the periphery of a circular tunnel for which the rock displacement is

$$U_r = U_{ro} r_o \frac{1}{x} \tag{3}$$

where x is the radius at any point, r_o is the radius of the tunnel, and U_{ro} is the displacement at the tunnel wall which will change in dependence of the far-field stress and the rock properties. If the bolt is assumed rigid, from equilibrium considerations

$$U_x L = U_{ro} r_o \int_{r_o}^{r_o+L} \frac{1}{x} dx \tag{4}$$

and since, by definition, there is no relative slip at the neutral point

$$U_x = \frac{U_{ro} r_o}{\rho} = \text{const} \tag{5}$$

where ρ is the location of the neutral point. Substituting (5) into (4), evaluating the integral and rearranging gives

$$\rho = \frac{L}{\ln\left(\frac{r_o + L}{r_o}\right)} \tag{6}$$

Thus the location of the neutral point depends only on the dimensions of the problem.

Concerning the distribution of shear stress along the bolt, Yu and Xian,[10] and more particularly Indraratna and Kaiser,[11] who used the analysis in their treatment of the extent of yielding around circular tunnels reinforced with fully grouted rock bolts, present plots which incorrectly show a decrease in shear stress towards both ends of the bolt. In fact, since the cable is assumed rigid, the shear stress is given by

$$\tau_x = k U_{ro} r_o \left(\frac{1}{x} - \frac{1}{\rho}\right) \tag{7}$$

and therefore extreme values of shear stress occur at the two ends of the bolt. As will be shown below, only if the assumption of a rigid bolt is dropped this is not the case. Integrating equation (7) and using the condition: $F_x = 0$ at $x = r_o$, gives the distribution of axial force

$$F_x = k U_{ro} r_o \left\{ \ln\left(\frac{x}{r_o}\right) - \frac{1}{\rho}(x - r_o) \right\} \tag{8}$$

Analysis of a fully grouted elastic bolt

Let us now extend the analysis to the case when the bolt is assumed to be elastically deformable. Following Farmer,[5] the equilibrium of a fully grouted rock bolt may be written

$$A \delta \sigma_x = - F_s \delta x \tag{9}$$

or

$$\frac{d\sigma_x}{dx} = \frac{- F_s}{A} \tag{10}$$

where F_s is the shear force due to bond per unit length and A is the cross-sectional area of the bolt. Now, for an elastic bolt

$$\sigma_x = E_b \frac{dU_x}{dx} \tag{11}$$

hence substituting (11) into (10),

$$\frac{d^2 U_x}{dx^2} = \frac{-F_s}{AE_b} \tag{12}$$

Let us assume that the shear force due to bond for a unit length of bolt is a linear function of the relative slip between the bolt and the rock:

$$F_s = k(U_r - U_x) \tag{13}$$

for which, in general, k should be determined from the load–displacement response during a pull test. This formulation ignores shear of the borehole wall. Farmer[5] justifies the latter because for a resin grouted bolt, the modulus of elasticity of the rock is likely to be an order of magnitude greater than for the grout. For cement grouted bolts the same argument can be applied for hard rock, though not for soft rock. However, for the latter, debonding at the bolt–grout interface will likely pre-empt the development of significant shear deformation at the borehole wall.

Any function may be chosen to describe the distribution of $U_r(x)$ over the bolt length $(0 < x < L)$. In general, U_r will decrease with distance from the surface of the excavation. The form and rate of this will depend on the size and shape of the opening, the strength and structure of the rock mass and the stress redistribution occurring on excavation. In engineering practise, U_r can be determined routinely using either an extensometer or a borehole camera.

Combining equations (12) and (13), the distribution of displacement along the bolt is described by the second-order inhomogeneous linear differential equation

$$\frac{d^2 U_x}{dx^2} - \frac{k}{AE_b} U_x = -\frac{k}{AE_b} U_r \tag{14}$$

For $k > 0$, the general form of the solution to equation (14) is

$$U_x = c_1 e^{\alpha x} + c_2 e^{-\alpha x} + \frac{e^{\alpha x}}{2\alpha} \int e^{-\alpha x} U_r(x)\,dx - \frac{e^{-\alpha x}}{2\alpha} \int e^{\alpha x} U_r(x)\,dx \tag{15}$$

where

$$\alpha^2 = k/AE_b \tag{16}$$

and, c_1 and c_2 are constants which can be determined from the end conditions.

Notice that for $U_r(x) = 0$, this is essentially identical to the solution given by Farmer.[5] In this paper, we will presume that U_r can be represented by an analytical function of x along the length of the bolt $(0 < x < L)$. Firstly, suppose that the distribution of rock mass displacement is represented by a continuous function for $U_r(x)$. Aydan[9] obtained a solution to this equation for the case:

$$U_r = U_{ro} e^{-nx} \tag{17}$$

where U_{ro} is the displacement occurring at the wall of the excavation which will change in dependence of the far-field stress and the rock properties, and n is a constant.

In the Appendix, two additional solutions are presented for

$$U_r = U_{ro} r_o/(r_o + x) \tag{18}$$

and,

$$U_r = U_{ro} H(x - a) \tag{19}$$

The former is the same as that used by Yu and Xian[10] but with a shift in the x-co-ordinate. For this case, a solution for U_x can only be determined approximately using a series expansion for the value of the Exponential Integral (see the Appendix for details). In equation (19), $H(\,)$ is the Heaviside step function. This distribution of U_r is intended to simulate the effect of opening on a rock joint located at $x = a$.

For both cases the coefficients c_1 and c_2 are determined for two different end conditions, unplated and plated (see Figure 2). Figure 3 shows the distribution of bolt displacement, axial load and shear stress for $k = 1$, 10 and 100 N/mm for each. Notice that:

(i) Whereas at low k, the bolt tends to merely translate, at higher k it stretches, and as a result;
(ii) higher axial loads develop for higher k.
(iii) For the continuous function of U_r (Figure 3(a)), in contrast to the solution presented by Yu and Xian,[10] the location of the neutral point is now seen to be dependent on the bond stiffness, being closer to the free surface for higher k; and,
(iv) significantly higher axial loads are developed in the bolt for the step function (Figure 3(b)) when the strain in the rock is concentrated at a single point.

Figure 4 shows results corresponding to Figure 3(a) when a rigid faceplate is installed. The shear stress is zero at the plate and negative along the entire length of the bolt, so that in effect, the location of the plate and the neutral point are coincident. For the step function, the load distribution is dependent on the distance between the discontinuity and the plate. Figure 5 compares the load distribution in the bolt when the fracture is located at different distances from the free face, for both unplated and plated cases. Whereas the peak load in the bolt decreases when the fracture is close to the free face for the unplated case, it actually increases for the plated case.

These results provide insight into how this type of analysis might possibly be used to improve understanding of the behaviour of fully grouted bolts, and potentially to design bolt lengths. However, the principal assumption associated with the solutions presented above is that, according to equation (13), the relation between shear stress and relative slip is linear. Therefore, from a practical perspective, the analysis suffers from the same limitations as Farmer's solution,[5] in that they do not account for debonding at the bolt–grout interface. Although it would be possible to treat idealized non-linear bond strength analytically, as Aydan[9] did in his analysis, we have chosen to proceed, from here onwards, using a numerical approach.

NUMERICAL TREATMENT

Presuming that, within a given interval of the bolt length, the bolt displacement (U_x) varies quadratically, then the difference form of equation (14) may be written:

$$\frac{\dfrac{U_x^{i-1} - U_x^i}{x^{i+1} - x^i} - \dfrac{U_x^i - U_x^{i-1}}{x^i - x^{i-1}}}{\dfrac{x^{i+1} - x^{i-1}}{2}} - \frac{k}{AE_b} U_x^i = -\frac{k}{AE_b} U_r^i \tag{20}$$

where the superscript i refers to the ith nodal point (Figure 6). Upon rearrangement this can be written as

$$-\frac{AE_b}{x^i - x^{i-1}} U_x^{i-1} + \left(\frac{AE_b}{x^i - x^{i-1}} + \frac{AE_b}{x^{i+1} - x^i} + k\left(\frac{x^{i+1} - x^{i-1}}{2}\right)\right) U_x^i - \frac{AE_b}{x^{i+1} - x^i} U_x^{i+1}$$

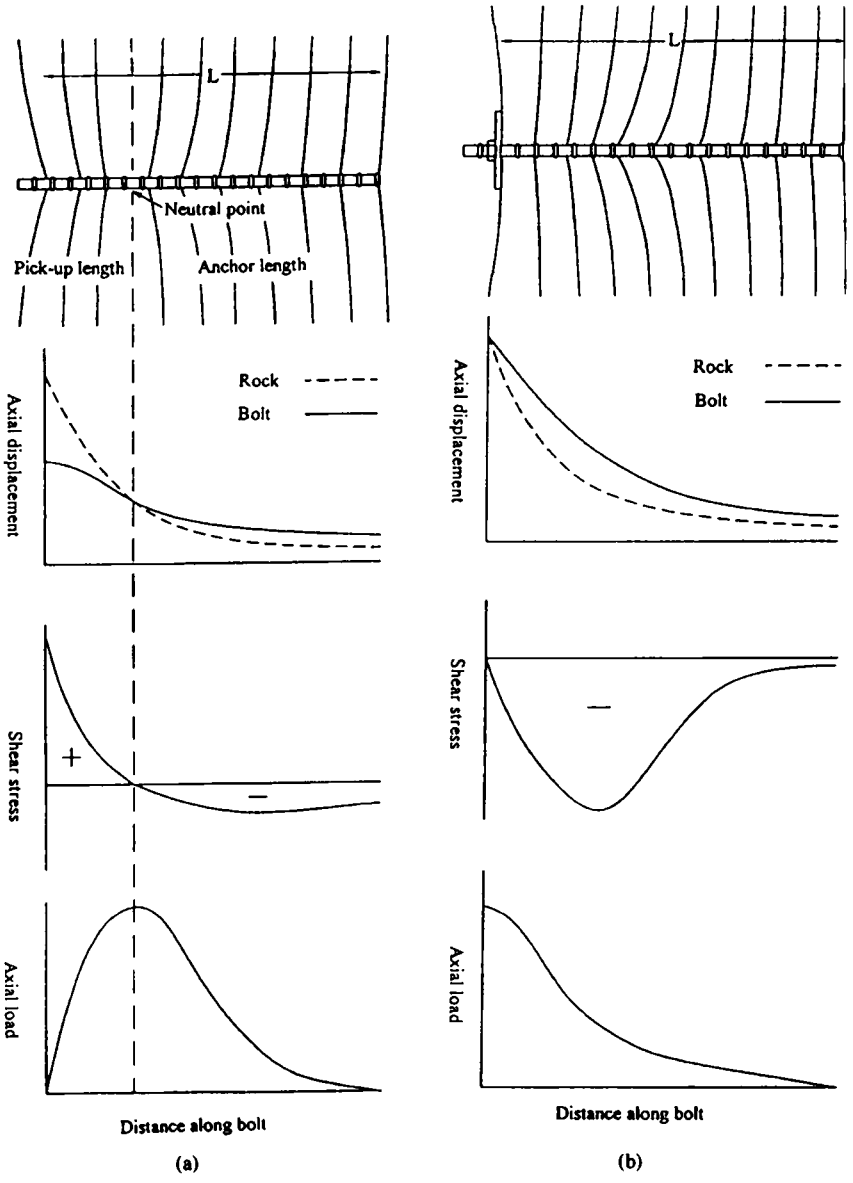

Figure 2. The two diffferent end conditions for the bolt problem: (a) two free ends, and (b) face plate attached at the excavation surface

$$= k\left(\frac{x^{i+1} - x^{i-1}}{2}\right)U_r^i \tag{21}$$

or more concisely,

$$-c^{i-1}U_x^{i-1} + \left(c^{i-1} + c^i + k\left(\frac{x^{i+1} - x^{i-1}}{2}\right)\right)U_x^i - c^iU_x^{i+1} = k\left(\frac{x^{i+1} - x^{i-1}}{2}\right)U_r^i \tag{22}$$

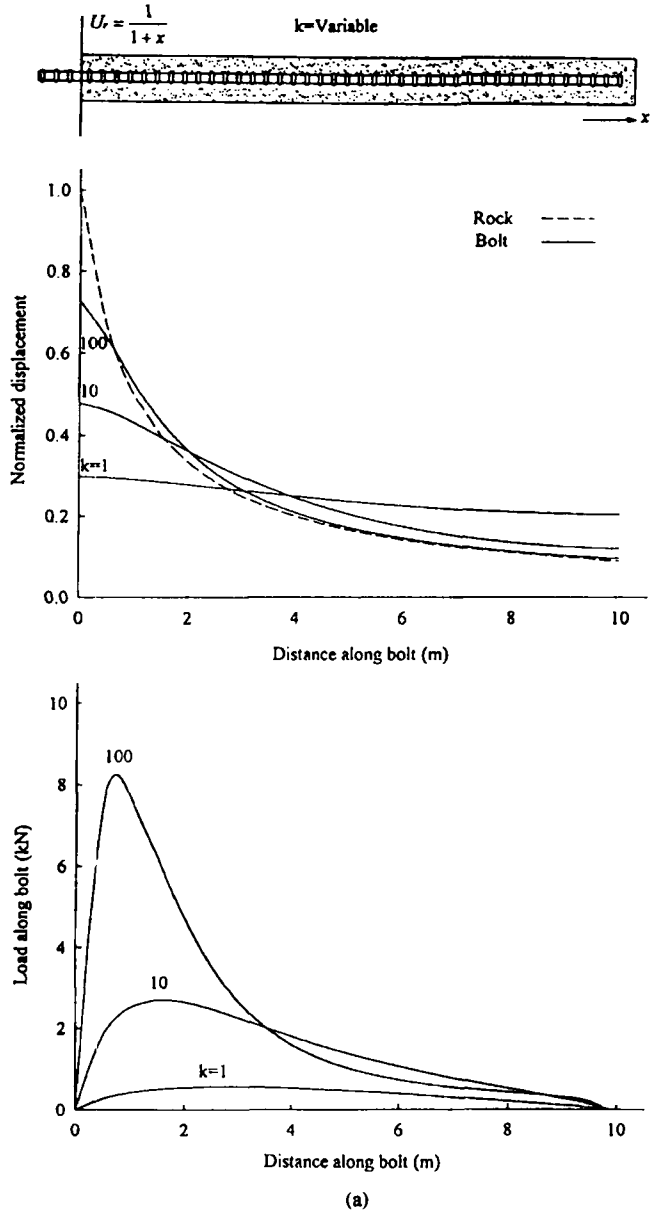

(a)

Figure 3. Analytical solutions for axial displacement (U_x) and axial load (F_x) for prescribed distributions of U_r: (a) Inverse function (equation (18)); (b) step function (equation (19)), for different values of k. Bolt has two free ends. All the solutions are for $U_{ro} = 1$ mm, and because both the bolt and the interface are linear, the result can be simply scaled for different displacements

where

$$c^i = AE_b/(x^{i+1} - x^i) \tag{23}$$

If the internodal spacing, l, is constant then

$$c^i = AE_b/l \tag{24}$$

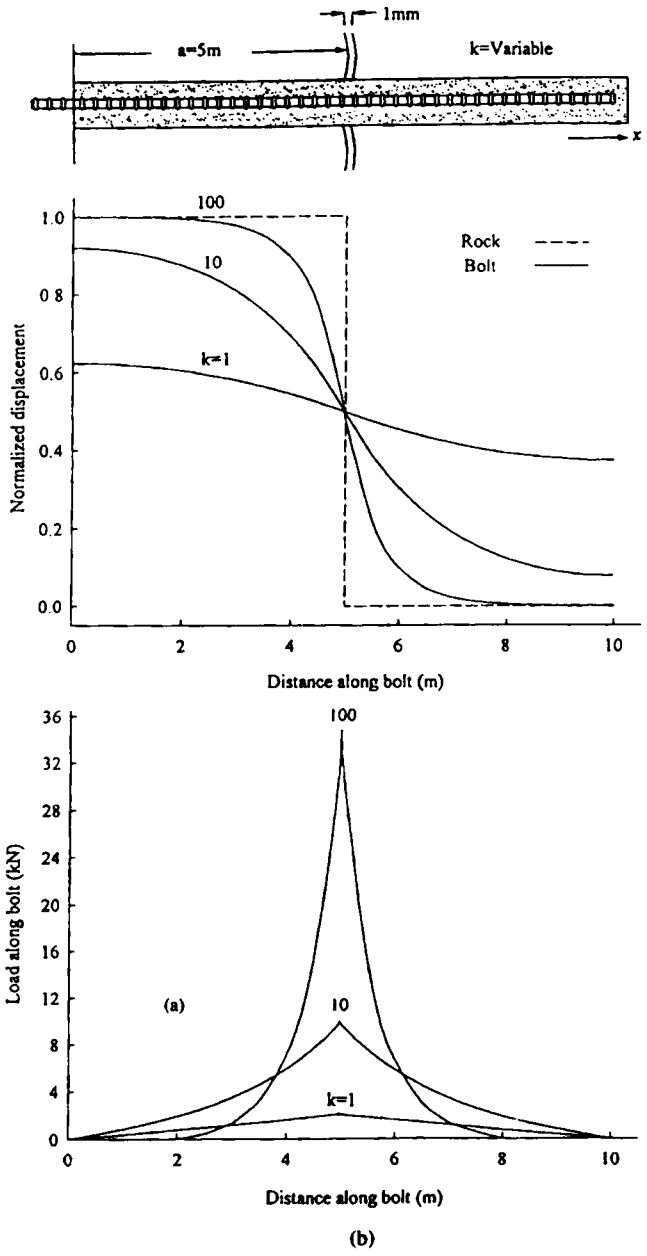

Figure 3. Continued.

For $i = 1$, the form of equation (22) depends on the end condition:
For a free end:

$$\left(c^1 + k\frac{x^2 - x^1}{2}\right)U_x^1 - c^1 U_x^2 = kU_{ro}\frac{x^2 - x^1}{2} \tag{25a}$$

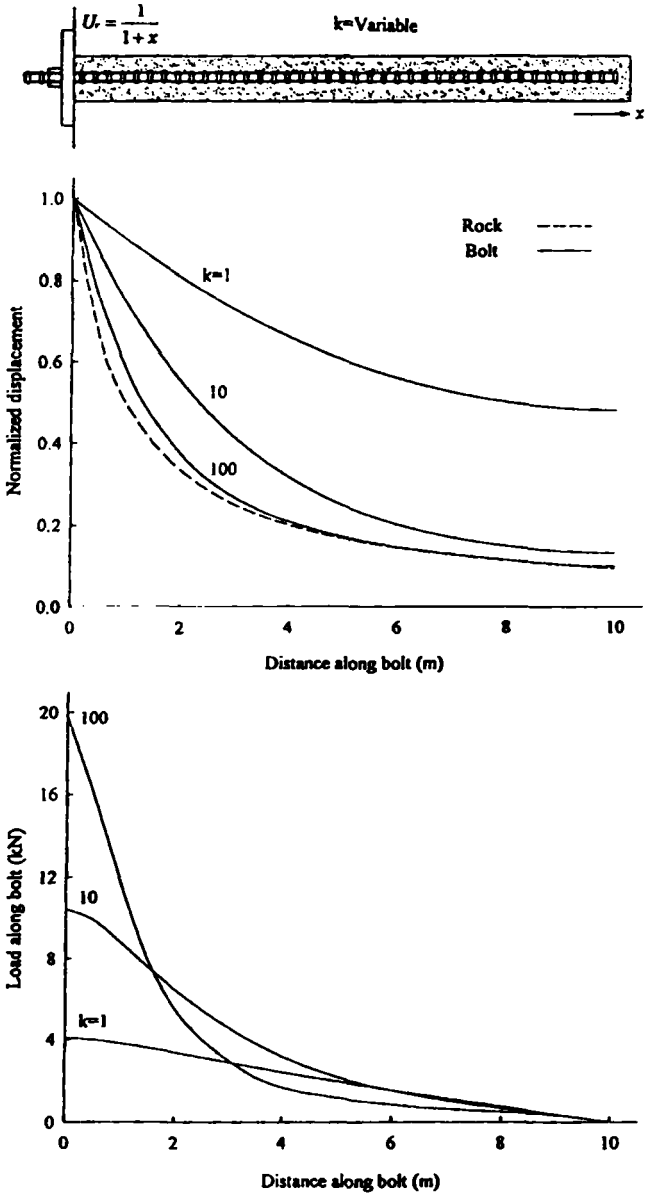

Figure 4. Analytical solutions for axial displacement (U_x) and axial load (F_x) for the inverse function of U_r with different values of k. Bolt has faceplate attached to one end

and with a faceplate installed, since $U_x^1 = U_{ro}$, and the reaction force applied by the faceplate, F_x^1, is unknown:

$$-F_x^1 - c^1 U_x^2 = -c^1 U_{ro} \tag{25b}$$

If the other end of the bolt corresponds to the nth nodal point

$$-c^{n-1} U_x^{n-1} + \left(c^{n-1} + k\frac{x^n - x^{n-1}}{2}\right) U_x^n = kU_r^n \frac{x^n - x^{n-1}}{2} \tag{26}$$

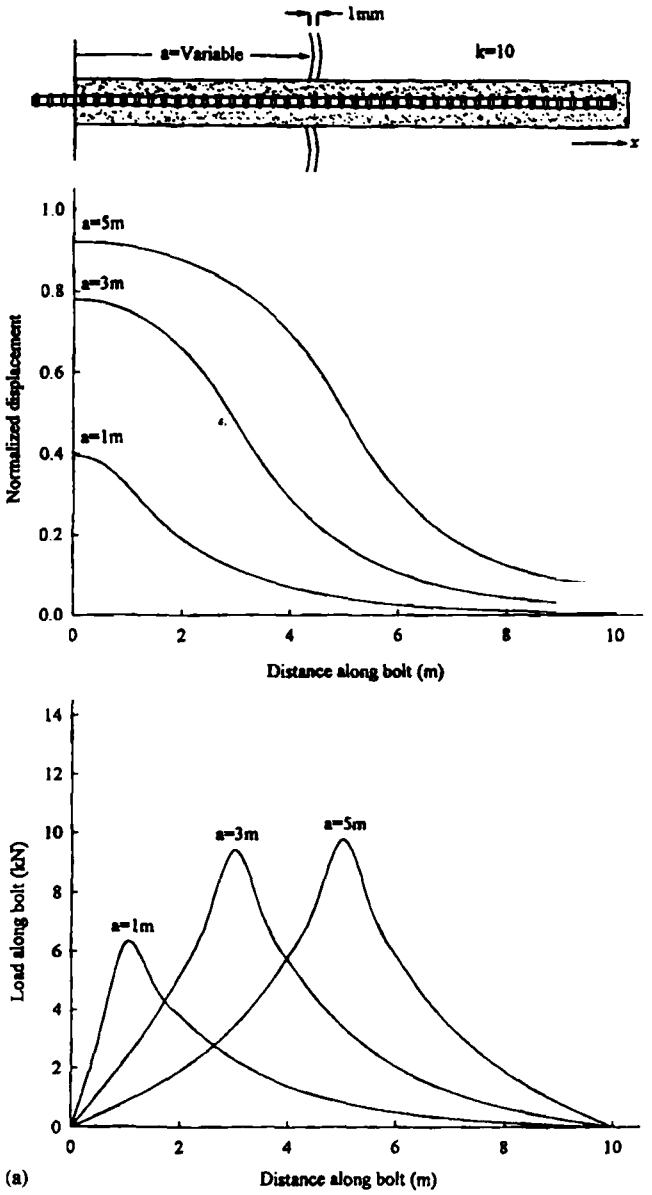

Figure 5. Analytical solutions showing the variation in axial load (F_x) as a in the Heaviside distribution $H(x-a)$ decreases. This is equivalent to reducing the distance between a dilatant joint and the free face (a) Two ends free, (b) faceplate applied

Equations (22), (25) and (26) comprise a matrix of n simultaneous equations, which when assembled in the correct order is tridiagonal in form, with n unknown values of U_x^*. The matrix can be solved directly, which because the number of nodes per bolt is typically < 20 is normally most efficient, or alternatively, by rearranging to obtain the out-of-balance force at each nodal

*This result can also be obtained using a finite element approach with constant strain elements (see Reference 13).

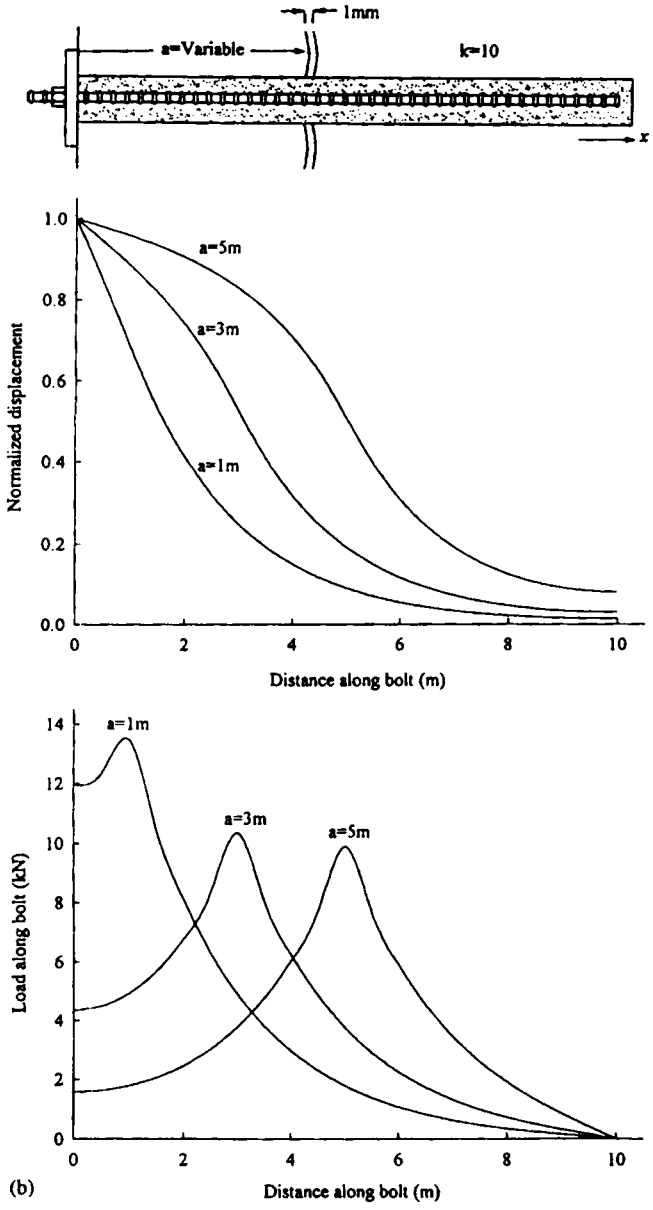

Figure 5. Continued.

point, solved using a relaxation method. Figure 7 compares the results obtained using this numerical technique with the analytical solutions derived earlier.

A NUMERICAL ANALYSIS OF THE LOAD AND DISPLACEMENT DISTRIBUTIONS ALONG FULLY GROUTED CABLE BOLTS

Until this point, the discussion has not specified a particular kind of bolt. However, the bond failure characteristics for the various types of bolt and grout are quite different. Therefore,

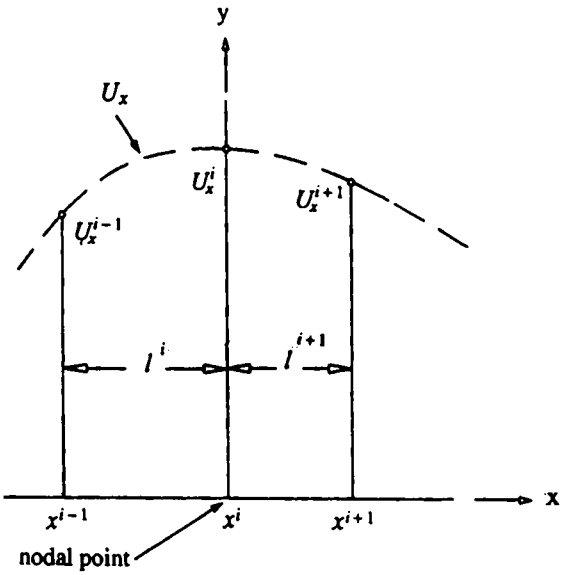

Figure 6. Notation for finite difference formulation

bearing in mind that the general approach holds for any type of bolt, the remaining discussion will be restricted to cement grouted cable bolts.

Cable bolting generally involves grouting a 15·2 mm (0·6″) helically would seven-wire strand cable using a portland cement paste into a 51–63 mm percussion drilled borehole. It is especially important for the pre-reinforcement of large underground excavations, and can be of critical importance to the economic viability of bulk mining methods for which considerable spans are opened. Since the cable is flexible and can be easily coiled, long lengths can be installed from relatively small development excavations, without the use of couplers (Figure 10). During subsequent mining, significant deformations, sometimes 50–100 mm, may cause the majority of the cable length to become debonded. In most cases involving collapse of cable reinforced ground, the bolts fail due to bond failure at the cable–grout interface rather than rupture of the steel. For some mines, the regularity of such failures raises doubts as to the cost-benefits of cable bolt reinforcement.

Bond strength of fully grouted cable bolts

Research[14–16] has established that the bond strength of fully grouted cable bolts may be regarded as frictional rather than adhesional in nature. Furthermore, as debonding proceeds, a progressive increase in the mismatch between the cable and the grout first splits the surrounding grout annulus, and thereafter pushes the resultant grout wedges aside. Depending on the stiffness of the borehole wall, a reaction pressure develops that controls the normal stress acting at the cable–grout interface where slip is occurring and hence the bond strength of the bolt. This behaviour was investigated by Hyett et al.[17] in a series of laboratory pull tests conducted in a modified Hoek cell. For these experiments, P, the radial pressure applied by the cell, and U_s, the slip at the cable–grout interface, were controlled (i.e. independent variables): F_s, the shear force due to bond for a unit length, and v, the radial dilation at the outside of the grout annulus were

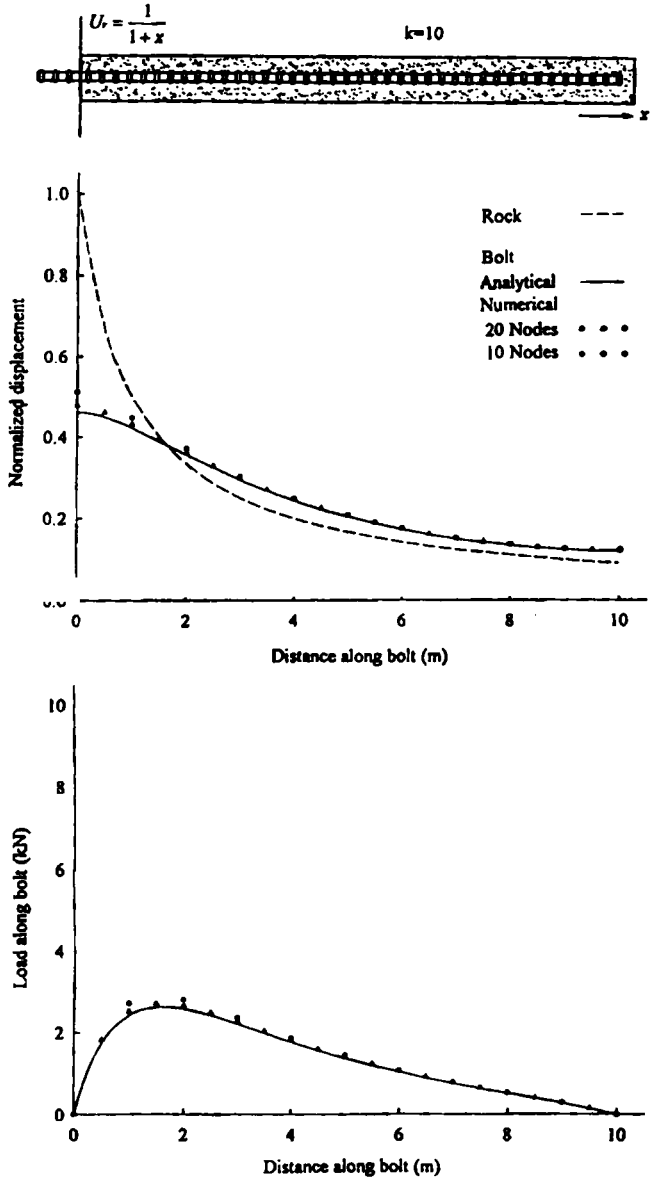

Figure 7. Comparison of finite difference and analytical solutions for the inverse distribution of rock displacement (equation (18)). The effect of different node spacings is shown

measured (i.e. dependent variables). Figure 8 shows a typical series of results for tests conducted at a range of different confining pressures. Each line is an average of 4–5 pull test results. As would be expected, at higher confining pressures, the bond strength is higher and the radial dilation is lower. The full suite of results were used to develop an elasto-plastic model for the shear force developed due to bond. In this

$$F_s = K_s U_s \tag{27}$$

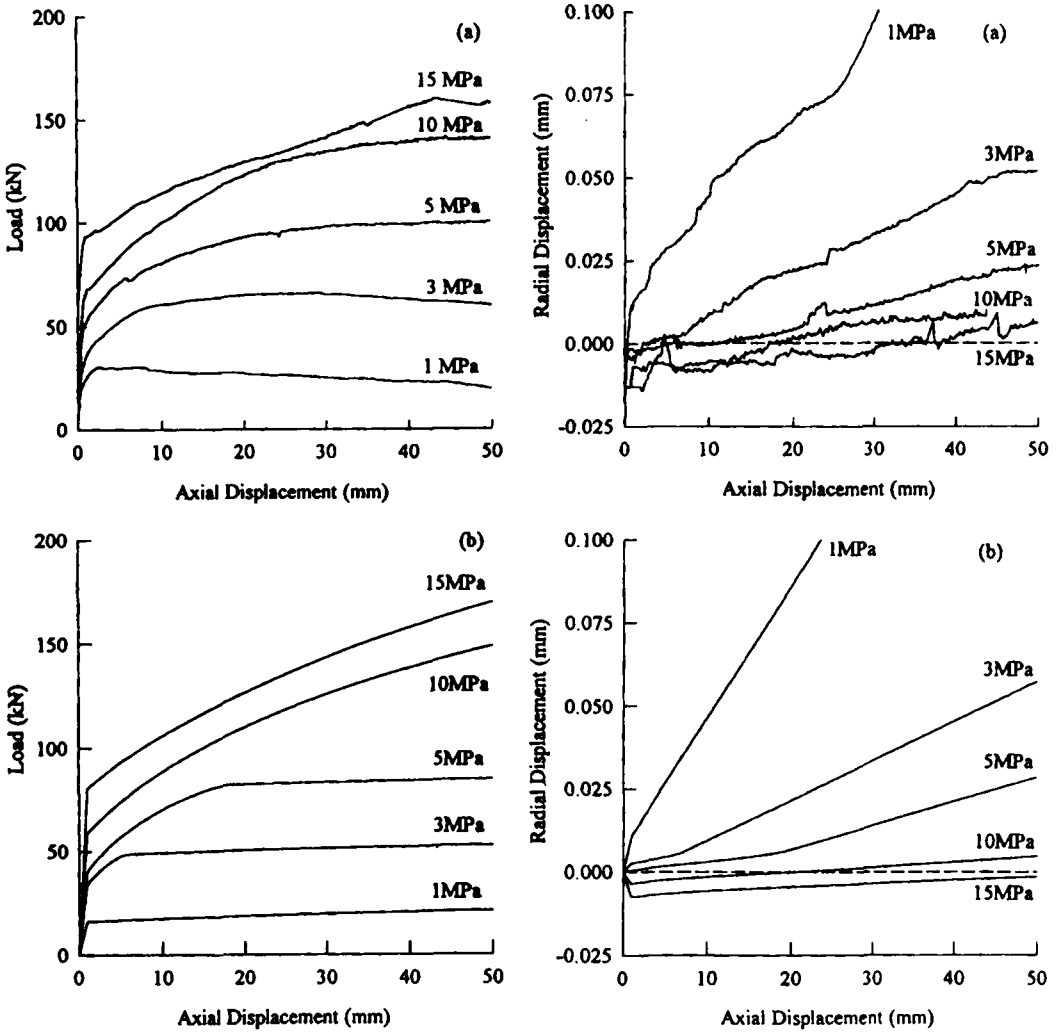

Figure 8. (a) Cable bolt (15.2 mm nominal diameter) pull test results conducted in a modified Hoek cell. LHS — axial load (F_a) versus axial displacement (U_a). RHS: dilation (v) versus axial displacement (U_a) (see Reference 16 for details). 0·3 $w:c$ ratio: 250 mm embedment length. (b) Simulations using the cable bolt model (equations (27)–(32). Values of P = const are shown on each curve

$$v = K_s P \tag{28}$$

where

$$K_s = F_p / U_b \tag{29}$$

and K_s is the radial stiffness of the cement annulus, and U_b is the limit of the initial stiff load-displacement response observed from Figure 8, and which based on experimental evidence is assumed to be a constant. When the shear force due to bond (F_s) described by (27) is equal to the bond capacity (F_p), bond slip and dilation occur. When $U_a = U_b$, F_p and v are given by

$$F_p = K_1 P \tag{30}$$

$$v = -K_s P + v_{sp} \tag{31}$$

and thereafter incrementally by

$$\begin{matrix} \mathrm{d}F_p \\ \mathrm{d}v \end{matrix} = \begin{bmatrix} K_1 & K_2 \\ K_3 & K_4 \end{bmatrix} \begin{matrix} \mathrm{d}P \\ \mathrm{d}U_a \end{matrix} \tag{32}$$

where $K_1, K_2, \ldots$, are coefficients relating the independent and dependent test variables, and which can be rearranged to form an incremental stiffness matrix, and v_{sp} is the radial dilation cuased by radial splitting of the grout annulus. As explained in detail by Hyett *et al.*,[17] $K_1, K_2, \ldots$ completely describe the non-linear frictional-dilational behaviour of the cable–grout interface, and account for the transfer of stress through, and deformability of, the fractured grout annulus. Consequently, they depend on parameters such as the nominal diameter of the cable, the grout water: cement ($w:c$) ratio (which can be related to the fundamental mechanical properties of the grout, E_g, v_g, etc.) and the borehole diameter.

Now, in practice the cable bolt system is radially confined. Let us assume that the effect of confinement can be represented using the elastic solution for a thick walled hollow cylinder in a triaxial stress field given by Obert and Duvall.[18] The incremental displacement at the inner surface $\mathrm{d}u_r$ may be written in terms of changes in the internal pressure ($\mathrm{d}p_i$), the external pressure ($\mathrm{d}p_o$) and the pressure acting coaxial with the cylinder ($\mathrm{d}p_z$)

$$\mathrm{d}u_r = \frac{(1+v)}{E}\left[\frac{\mathrm{d}p_i r_i^3 - \mathrm{d}p_o r_i r_o^2}{r_o^2 - r_i^2}(1-2v) - \frac{r_i r_o^2}{r_o^2 - r_i^2}(\mathrm{d}p_o - \mathrm{d}p_i)\right] + \frac{v}{E} r_i \left(\mathrm{d}p_z + 2v \frac{\mathrm{d}p_i r_i^2 - \mathrm{d}p_o r_o^2}{r_o^2 - r_i^2}\right) \tag{33}$$

where r_i and r_o are the inner and outer radii respectively, and E and v are elastic constants. To satisfy continuity at the grout–confinement interface, $\mathrm{d}u_r$ and $\mathrm{d}p_i$ in equation (33) must equal $\mathrm{d}v$ and $\mathrm{d}P$ in equation (32) and hence the two equations may be combined to predict the load developed during bond failure. For conciseness, let us consider the result for two special cases. First, when the confinement is provided by a pipe during a laboratory pull test (i.e. $p_o = p_z = 0$, r_i is the inner radius of the pipe, r_o the outer radius):

$$\mathrm{d}F_p = \left(\frac{K_4 K_1 K_p}{1 - K_3 K_p} + K_2\right)\mathrm{d}U_a \tag{34}$$

in which K_p the radial stiffness of the pipe is given by

$$K_p = E\left\{\frac{r_o^2 - r_i^2}{r_i[(1-v)r_i^2 + (1+v)r_o^2]}\right\} \tag{35}$$

Figure 9 compares cable bolt pull test results for a 250 mm embedment length, conducted in confining tubes of different radial stiffness for a 0.3 $w:c$ ratio grout, with those predicted by the model based on equation (34). Second, when the confinement is provided by a borehole wall within a rock mass subjected to excavation induced stress change tensor with principal components $\mathrm{d}\sigma_{r1}$, $\mathrm{d}\sigma_{r2}$ and $\mathrm{d}\sigma_z$, the latter acting coaxial with the borehole. Since when $r_o \to \infty$, $\mathrm{d}p_o$ in equation (33) becomes equivalent to $\mathrm{d}\sigma_r$, the mean far-field (relative to the cable bolt hole) radial stress change, and $\mathrm{d}p_z$ becomes equivalent to $\mathrm{d}\sigma_z$, equation (33) reduces to

$$\mathrm{d}u_r = \frac{(1+v_r)R}{E_r}\mathrm{d}p_i - \frac{2R}{E_r}\mathrm{d}\sigma_r + \frac{v_r}{E_r}\mathrm{d}\sigma_z \tag{36}$$

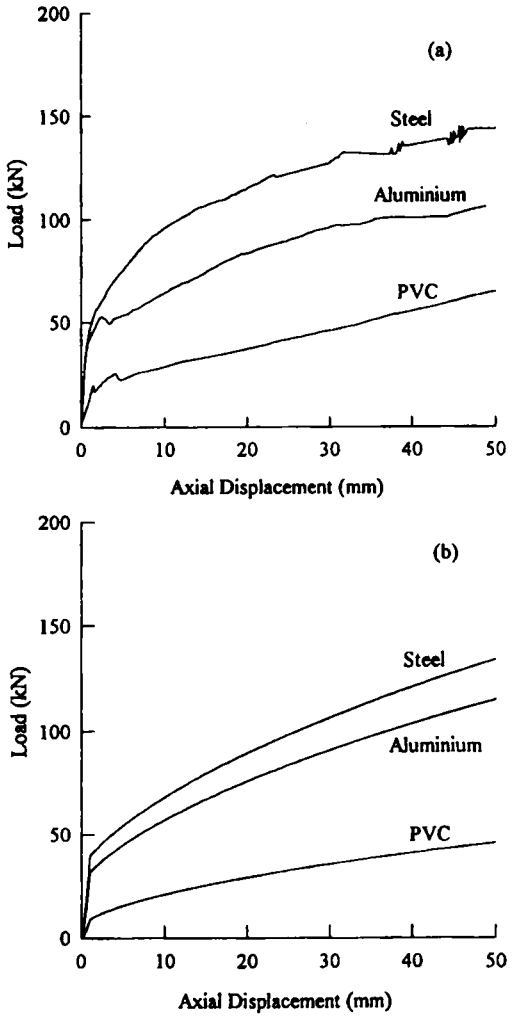

Figure 9. (a) Laboratory cable bolt pull test results conducted in steel (K_p = 1640 MPa/mm), aluminium (599 MPa/mm) and PVC (322 MPa/mm) confining pipes. $w:c$ ratio of grout is 0·3. (b) Simulation using equation (34)

where E_r and ν_r are the Young's modulus and Poisson's ratio of the rock on a scale pertaining to the cable bolt hole of radius R. Then,

$$dF_p = \left(\frac{K_4 K_1 K_r}{1 - K_3 K_r} + K_2\right) dU_a + \frac{2K_1}{(1 - K_3 K_r)(1 + \nu_r)} d\sigma_r - \frac{K_1 \nu_r}{(1 - K_3 K_r)(1 + \nu_r)} d\sigma_z \quad (37)$$

in which K_r, the radial stiffness of the borehole wall, is given by

$$K_r = \frac{dp_i}{du_r} = \frac{E_r}{(1 + \nu_r)R} \quad (38)$$

Equation (37) can be written more generally as

$$dF_p = K_U dU_a + K_\sigma d\sigma \quad (39)$$

Load distribution along fully grouted cable bolts

During bond failure, $F_s = F_p$, and therefore equation (39) can be substituted into (12). Realising also that U_s for a pull test is equivalent to the relative slip U_r–U_x of the bolt, and writing the difference form of the resulting differential equation yields:

$$-c^{i-1}\,\mathrm{d}U_x^{i-1} + \left(c^{i-1} + c^i + K_U^i\left(\frac{x^{i+1} - x^{i-1}}{2}\right)\right)\mathrm{d}U_x^i - c^i\,\mathrm{d}U_x^{i+1}$$
$$= \left(\frac{x^{i+1} - x^{i-1}}{2}\right)[K_U^i\,\mathrm{d}U_r^i + K_\sigma^i\,\mathrm{d}\sigma^i] \tag{40}$$

for the ith nodal point, in which $\mathrm{d}U_r$ and $\mathrm{d}\sigma$ are indexed in recognition that they may vary throughout the problem domain. Proceeding as for the linear bond case presented in the previous section, a series of simultaneous equations can be constructed, which when solved to describe the incremental change in axial displacement (U_x) and axial load (F_x) along a linear elastic cable, caused by known increments of rock mass displacement and excavation induced stress change. Of course, within the rock mass, U_r and σ will be inter-related: they will also be affected by the reinforcing action of the cable bolts themselves. However as for the analytical treatment above, these interactions are ignored. Therefore, strictly speaking, the results apply to cases for which the displacements and stresses within the cable bolted domain have been either independently measured (i.e. using stress cells and extensometers, respectively) or can be estimated. This can still be of considerable practical benefit because although instrumentation to measure rock mass displacements is commercially available and widely used, that to measure bolt load is not.

Effect of rock mass displacement profile

Figure 10 shows how the distribution of axial load developed, for a 10 m cable bolt installed, without a faceplate, into the wall of an excavation which has progressively displaced according to equations (18) and (19). For the continuous distribution of rock mass displacement, even for $U_{ro} = 50$ mm, the maximum load in the cable is only 200 kN. In contrast, for the step function, in which the change in rock mass displacement (i.e. the rock mass strain) is concentrated at a point, the load in the cables develops to the ultimate strength of the cable at $U_{ro} = 20$ mm. For multiple steps in the rock mass distribution, the axial load exhibits multiple maxima, and the axial load developed in the cable is intermediate between the continuous distribution and the single step. These results demonstrate the critical importance of rock mass structure in determining the response of a fully grouted cable bolt. Many engineers believe that the stiffness of a reinforcing system is a property of the reinforcement alone. In fact, for fully grouted reinforcement systems, stiffness, which can be thought of as increase of load in the reinforcement system for an increment of rock mass displacement, is dependent on the distribution of strain in the rock, and therefore on rock mass structure. If all other things are equal, a fully grouted reinforcement system will be stiffer if the strain in the rock mass is concentrated at a few points (i.e. at rock joints which are opening) than if it is more evenly distributed.

Effect of rock mass modulus and excavation induced stress change

Figure 11 shows the distribution of load in a 10 m cable, for $U_{ro} = 50$ mm, with different values of E_r which controls borehole wall stiffness. The effect is relatively limited over the range of likely

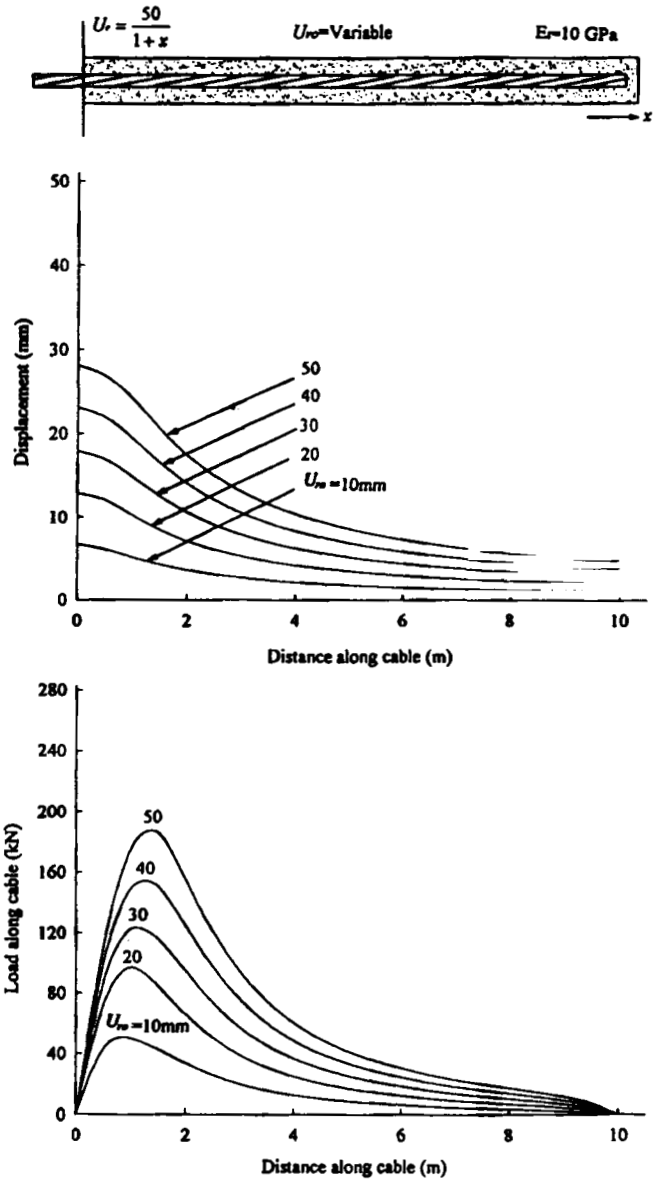

Figure 10. Axial displacement and load distribution along a 10 m cable bolt (15·2 mm nominal diameter) for a 10 GPa (ν_r = 0·25) rock with different distributions of rock mass displacement. 0·3 *w:c* ratio grout. Borehole diameter is 57 mm

values. This is because, as indicated in Figure 9, the effect of rock mass modulus on bond strength increases with axial displacement (i.e. relative slip), and along the majority of the cable length even at U_{ro} = 50 mm, the relative slip is < 5 mm.

However, E_r, through K_r, also determines the effect of stress change on the cable bolt bond strength. Figure 12 shows the effect of a hydrostatic stress change along the entire cable length occurring during rock mass displacement for E_r = 10 and 100 GPa. By far the most dramatic effect of excavation induced stress change on axial load was for E_r = 10 GPa. This result suggests

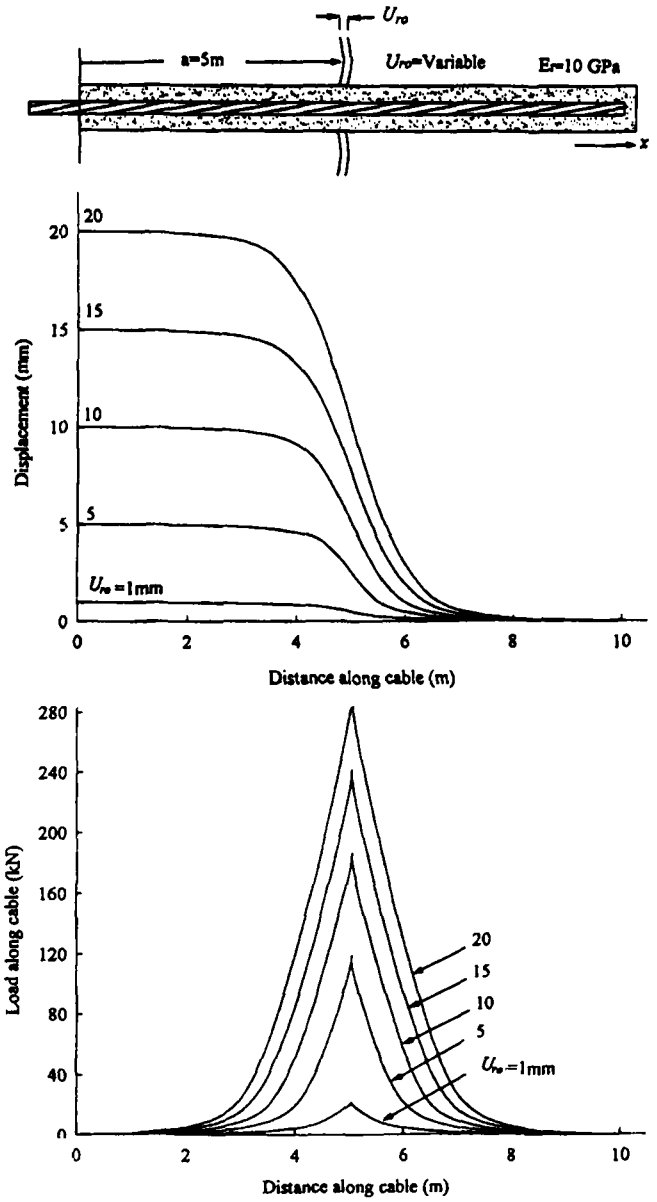

Figure 10. Continued.

that the combination of an excavation induced stress decrease and a poor quality (low E_t) rock mass may result in the development of very low axial load along the cable (due to the low bond capacity), potentially facilitating ground failure.

CONCLUSION

Based on a comparison of their own *in situ* instrumentation results in hard rock and Freeman's[3] results in a soft rock, Bjornfot and Stephansson[2] concluded that the major difference between

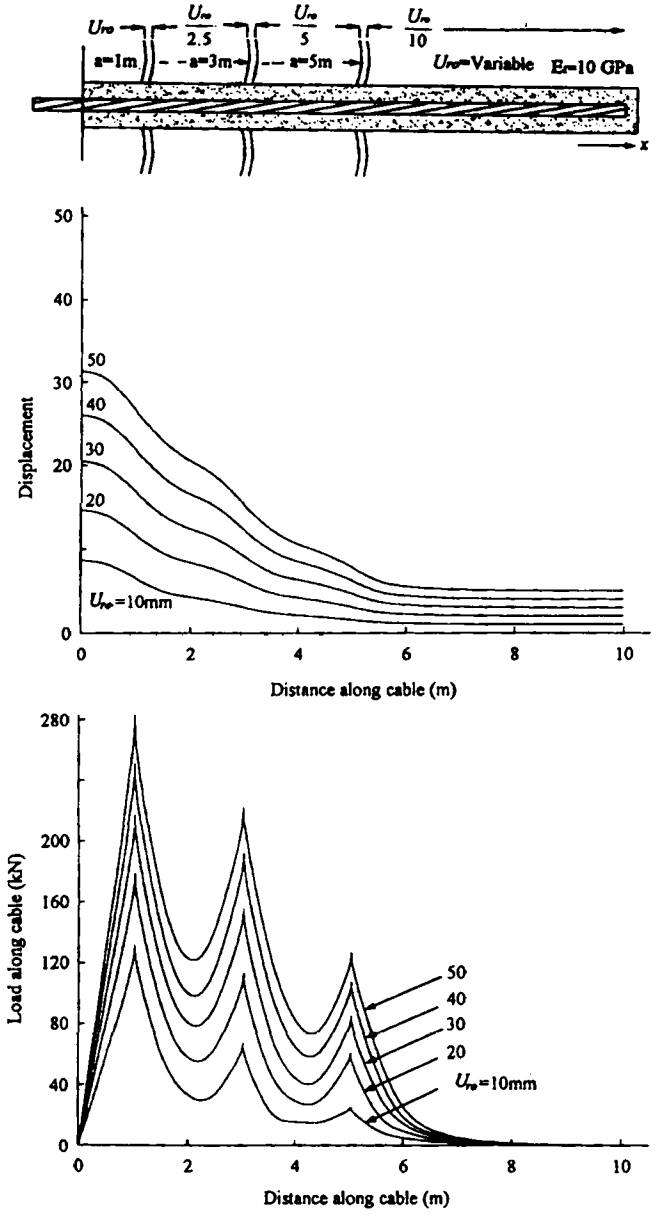

Figure 10. Continued.

rock bolting in hard and soft rock is as follows: 'In soft rocks, the relative displacement between the rock and the bolt induces longitudinal shear stress on the bolt, and one part forms the anchoring part, while the other end towards the opening forms the pick-up part. In hard masses of rock blocks, the shear stress reaches its maximum at the intersection with a major discontinuity. Away from the intersection the shear stresses in the bolt gradually diminish'. The analytical and numerical results presented in this paper confirm these differences. Furthermore, they indicate

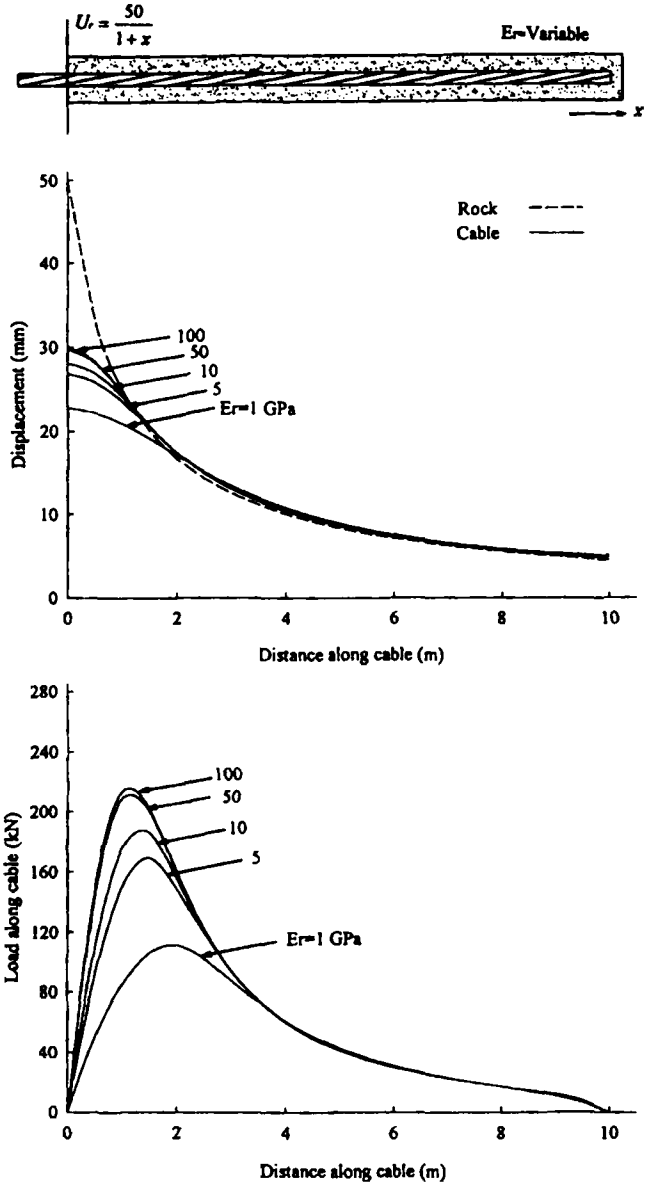

Figure 11. Effect of E_r on the axial displacement and load distribution along a 10 m cable bolt. 0·3 $w:c$ ratio. Other parameters identical to Figure 10

that for a specified bond stiffness, the maximum axial load developed in the bolt for discontinuous distribution of rock mass displacement is significantly higher than for the continuous distribution. For cement grouted cable bolt reinforcement, it has been shown that this effect, in combination with the sensitivity of bond stiffness to the radial confinement at the borehole wall, can explain frequently reported failures of cable bolted ground involving debonding at the cable–grout interface in soft rock, and why the only instances of cable rapture are confined to hard, blocky rock masses. Although the mechanics of bond failure may be somewhat different,

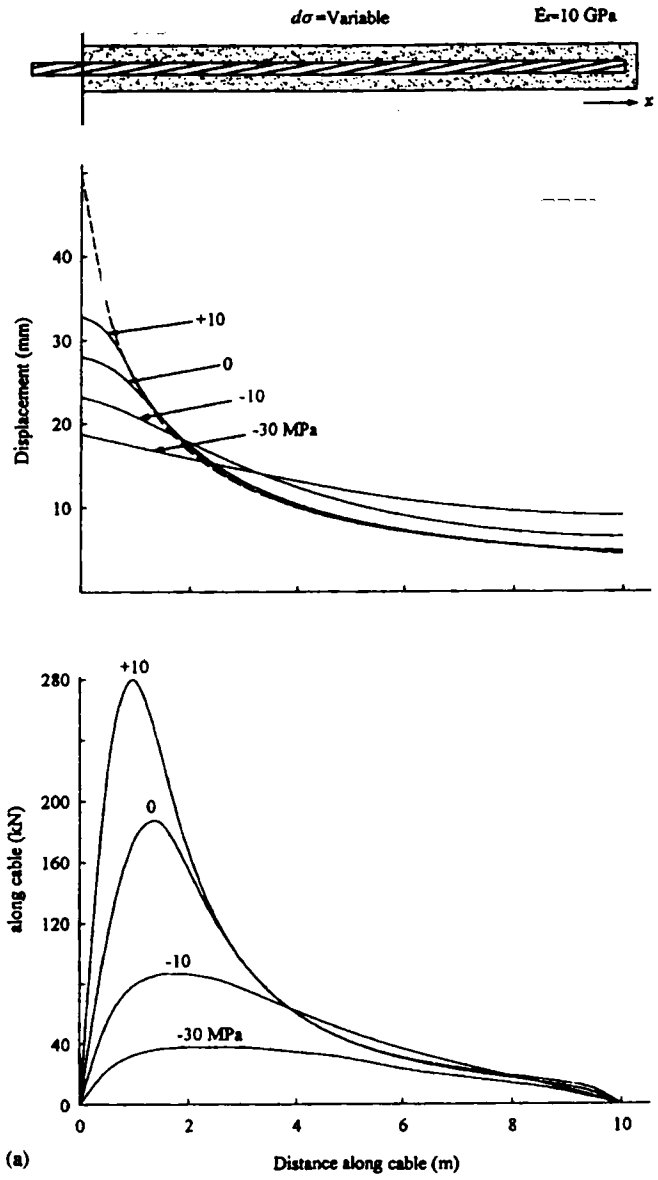

similar effects are predicted for other kinds of fully grouted reinforcement, potentially explaining the widely reported observation[19] that 'fully grouted rock reinforcement is more effective in hard rocks containing joints'.

This paper has purposely avoided the more complex considerations associated with rock mass–reinforcement interaction. However, an increasing number of numerical stress analysis packages have the capability to simulate fully grouted reinforcement. Their potential for reinforcement design, especially as three-dimensional analyses become feasible, should not be

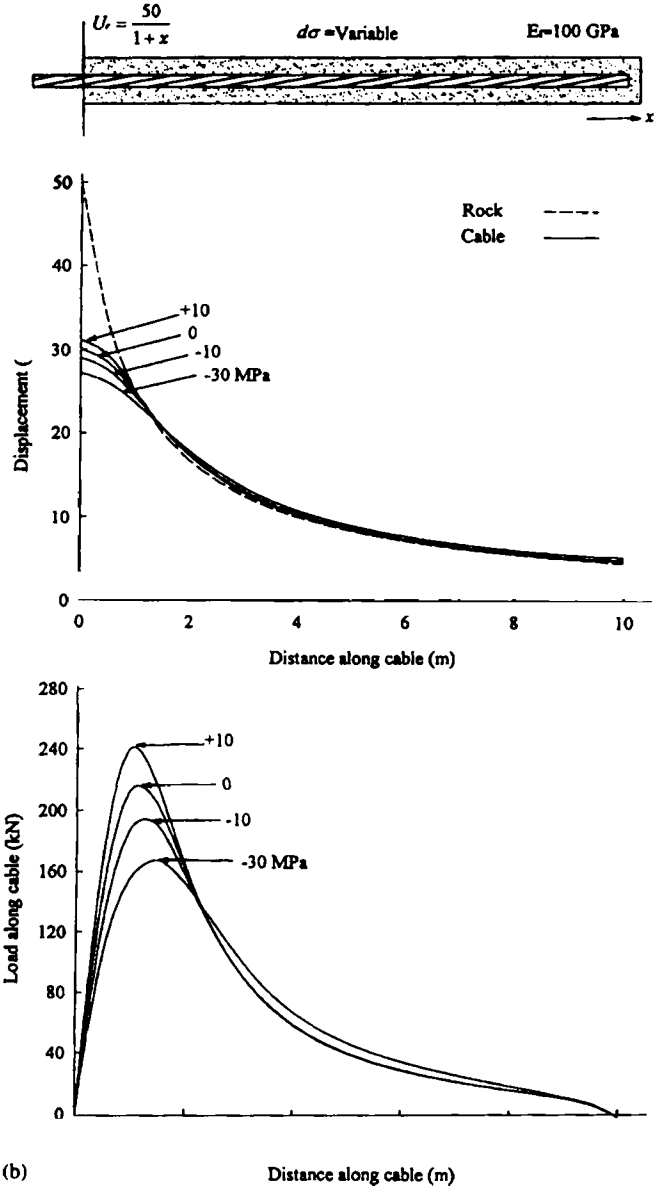

underestimated. This paper provides a guideline for the interpretation of these analyses, and, in particular, it emphasizes the importance of realistically representing both:

(i) the magnitudes of rock mass displacement and the pattern of rock mass strain; and,
(ii) the bond failure characteristics of the fully grouted reinforcement system used.

If two numerical models, one a discontinuum model, the other a continuum model predict the same magnitude of rock mass displacement at the free face, it has been demonstrated that higher

reinforcement loads will develop in the former. Therefore, if both models are used to simulate the rock mass–reinforcement interaction, the rock mass displacements predicted will tend to be reduced less in the continuum than in the discontinuum model.[19]

ACKNOWLEDGEMENTS

The authors gratefully acknowledge the constructive comments of two anonymous referees.

APPENDIX: ANALYTICAL SOLUTION FOR A CONTINUOUS AND DISCONTINUOUS FUNCTION OF ROCK DISPLACEMENT

Inverse variation of rock displacement with distance from the face

The distribution of rock mass displacements is given by

$$U_r = \frac{U_{ro} r_o}{(r_o + x)} \tag{41}$$

Substituting this in equation (14) gives the second-order differential equation to be solved:

$$\frac{d^2 U_x}{dx^2} - \alpha^2 U_x = -\alpha^2 \frac{U_{ro} r_o}{(r_o + x)} \tag{42}$$

This has the solution

$$U_x = \frac{U_{ro} r_o \alpha}{2} [\mathrm{EI}(\alpha(r_o + x))\, e^{\alpha(r_o + x)} - \mathrm{EI}(-\alpha(r_o + x))\, e^{-\alpha(r_o + x)}] + c_1 e^{\alpha x} + c_2 e^{-\alpha x} \tag{43}$$

EI(x) being the principal component of the Exponential Integral:

$$\mathrm{EI}(x) = -\int_{+x}^{\infty} \frac{e^{-t}}{t}\, dt = \int_{+x}^{-\infty} \frac{e^{t}}{t}\, dt \tag{44}$$

which can be evaluated using the series approximation

$$\mathrm{EI}(x) = -\ln|x| - \gamma - \left[\frac{-x}{1 \cdot 1!} + \frac{(-x)^2}{2 \cdot 2!} + \frac{(-x)^3}{3 \cdot 3!} \cdots \frac{(-x)^n}{n \cdot n!}\right] \tag{45}$$

where γ is Euler's constant (0·5772156 ...)

The corresponding value for axial force is

$$F_x = -AE_b \frac{U_{ro} r_o \alpha^2}{2} [\mathrm{EI}(\alpha(r_o + x))\, e^{\alpha(r_o + x)} + \mathrm{EI}(-\alpha(r_o + x))\, e^{-\alpha(r_o + x)}] + \alpha c_1 e^{\alpha x} - \alpha c_2 e^{-\alpha x} \tag{46}$$

Case 1: Two free ends.

For two free ends $F_x = 0$ at $x = 0$ and $F_x = 0$ at $x = L$, and thus

$$c_1 = \frac{U_{ro} r_o \alpha}{2} \left[\frac{\{\mathrm{EI}(-\alpha r_o) + \mathrm{EI}(-\alpha(r_o + L))\} e^{-\alpha(r_o + L)} + \mathrm{EI}(\alpha r_o)\, e^{\alpha(r_o - L)} - \mathrm{EI}(\alpha(r_o + L))\, e^{\alpha(r_o + L)}}{e^{\alpha L} - e^{-\alpha L}}\right] \tag{47a}$$

$$c_2 = \frac{U_{ro} r_o \alpha}{2}\left[\frac{\{\mathrm{EI}(\alpha r_o) - \mathrm{EI}(\alpha(r_o + L))\}e^{\alpha(r_o+L)} + \mathrm{EI}(-\alpha r_o)e^{-\alpha(r_o-L)} - \mathrm{EI}(-\alpha(r_o+L))e^{-\alpha(r_o+L)}}{e^{\alpha L} - e^{-\alpha L}}\right] \tag{47b}$$

Case 2: Faceplate attached to one end.
If a faceplate is attached to one end: $U_x = U_{ro}$ at $x = 0$ and $F_x = 0$ at $x = L$, whence

$$c_1 = \frac{U_{ro} r_o \alpha}{2} \times \left[\frac{\{\mathrm{EI}(-\alpha r_o) - \mathrm{EI}(-\alpha(r_o+L))\}e^{-\alpha(r_o+L)} - \mathrm{EI}(\alpha r_o)e^{\alpha(r_o-L)} - \mathrm{EI}(\alpha(r_o+L))e^{\alpha(r_o+L)} + 2U_{ro}e^{-\alpha L}}{e^{\alpha L} + e^{-\alpha L}}\right] \tag{48a}$$

$$c_2 = \frac{U_{ro} r_o \alpha}{2} \times \left[\frac{\{-\mathrm{EI}(\alpha r_o) + \mathrm{EI}(\alpha(r_o+L))\}e^{\alpha(r_o+L)} + \mathrm{EI}(-\alpha r_o)e^{-\alpha(r_o-L)} + \mathrm{EI}(-\alpha(r_o+L))e^{-\alpha(r_o+L)} + 2U_{ro}e^{-\alpha L}}{e^{\alpha L} + e^{-\alpha L}}\right] \tag{48b}$$

Step function of rock displacement with distance from the face

The differential equation to be solved is

$$\frac{d^2 U_x}{dx^2} - \alpha^2 U_x = -\alpha^2 U_{ro} H(x - a) \tag{49}$$

Applying the Laplace transform

$$s^2 V(s) - s U_x(0) - \frac{d}{dy} U_x(0) - \alpha^2 Y(s) = \alpha^2 U_{ro}\left(\frac{-e^{-as}}{s} + \frac{1}{s}\right) \tag{50}$$

Case 1: Two free ends.
Proceeding first for the condition of two free ends: since

$$\frac{d}{dy} U_x(0) = 0$$

$$V(s) = \frac{U_{ro}\alpha^2 e^{-as}}{s(s^2 - \alpha^2)} - \frac{U_{ro}\alpha^2}{s(s^2 - \alpha^2)} + \frac{s}{s^2 - \alpha^2} U_x(0) \tag{51}$$

Applying the inverse transform and maintaining $y(0)$ as an unknown constant

$$U_x = -U_{ro} H(x - a)(1 - \cosh(\alpha(x - a))) + U_{ro}(1 - \cosh(\alpha x)) + \cosh(\alpha x) U_x(0) \tag{52}$$

Differentiating and knowing that $dU_x/dx = 0$ at $x = L$ gives

$$\frac{d}{dx} U_x = \alpha U_{ro} H(x - a)\sinh(\alpha(x - a)) - \alpha \sinh(\alpha x)(U_{ro} - U_x(0)) = 0 \tag{53}$$

and thus

$$U_x(0) = U_{ro}\frac{\sinh(\alpha(-L+a)) + \sinh(\alpha L)}{\sinh(\alpha L)} \tag{54}$$

Substituting in equation (53) gives the final form for the displacement distribution

$$U_x = -U_{ro}H(x-a)(1-\cosh(\alpha(x-a))) + U_{ro}(1-\cosh\alpha x)\frac{\sinh(\alpha(-L+a)) + sinh(\alpha L)}{\sinh(\alpha L)} \tag{55}$$

and the force distribution

$$F_x = AE_b\left[\alpha U_{ro}(H(x-a)\sinh(\alpha(x-a)) - \sinh(\alpha x)\frac{\sinh(\alpha(-L+a)) + \sinh(\alpha L)}{\sinh(\alpha L)}\right] \tag{56}$$

Case 2: Faceplate attached to one end. Using equation (50) and knowing that $U_x(0) = U_{ro}$ at $x = 0$

$$V(s) = \frac{U_{ro}\alpha^2 e^{-as}}{s(s^2-\alpha^2)} - \frac{U_{ro}\alpha^2}{s(s^2-\alpha^2)} + \frac{U_{ro}s}{s^2-\alpha^2} + \frac{(dU_x(0)/dx)}{s^2-\alpha^2} \tag{57}$$

Applying the inverse transform

$$U_x = U_{ro}H(x-a)(1-\cosh(\alpha(x-a))) + U_{ro}(1-\cosh(\alpha x)) + U_{ro}\cosh(\alpha x) + \frac{(dU_x(0)/dx)}{\alpha}\sinh(\alpha x) \tag{58}$$

which simplifies to

$$U_x = U_{ro} - U_{ro}H(x-a)(1-\cosh(\alpha(x-a) + \frac{(dU_x(0)/dx)}{\alpha}\sinh(\alpha x) \tag{59}$$

Differentiating to obtain dU_x/dx, and using the boundary condition $dU_x/dx = 0$ at $x = L$, $dU_x(0)/dx$ can be found

$$\frac{dU_x(0)}{dx} = -U_{ro}\alpha\frac{\sinh(L-a)}{\cosh(\alpha L)} \tag{60}$$

Substituting (69) into equation (59) gives the solution for axial displacement:

$$U_x = -U_{ro}H(x-a)(1-\cosh(\alpha(x-a))) + U_{ro}\frac{\sinh(\alpha(-L+a))}{\cosh(\alpha L)}\sinh(\alpha x) \tag{61}$$

and for axial force

$$F_x = -AE_b\left[U_{ro}\alpha(H(x-a)\sinh(\alpha x-a)) - \cosh(\alpha x)\frac{\sinh(\alpha(-L+a))}{\sinh(\alpha L)}\right] \tag{62}$$

REFERENCES

1. E. Hoek and E. T. Brown, *Underground Excavations in Rock*, Institute of Mining and Metallurgy, London, 1980.
2. F. Bjornfot and O. Stephansson, 'Interaction of grouted rock bolts and hard rock masses at variable loading in a test drift of the Kiirunavaara Mine, Sweden', in Stephansson O. (ed.), *Proc. Int. Symp. Rock Bolting*, Abisko, 1983, pp. 377–395.

3. T. J. Freeman, 'The behaviour of fully grouted bolts in the Kielder experimental tunnel', *Tunnels Tunneling*, **10**, 37–40 (1978).
4. P. G. Fuller, 'Cable support in mining – a keynote lecture'. in O. Stephansson (ed.), *Proc Int. Symp. Rock Bolting*, Abisko, 1983, pp. 511–522.
5. I. W. Farmer, 'Stress distribution along a resin grouted rock anchor', *Int. J. Rock Mech. Min. Sci. Geomech. Abstr.*, **12**, 347–351 (1975).
6. O. Aydan, Y. Ichikawa and T. Kawamoto, 'Load bearing capacity and stress distribution in/along rockbolts with inelastic behaviour of interfaces', *Proc. 5th Int. Conf. Numercal Methods in Geomechanics*, Nagoya, 1985, pp. 1281–1292.
7. C. M. St. John and D. F. Van Dillen, 'Rockbolts: A new numerical representation and its application in tunnel design', *Proc. 24th U.S. Symp. Rock Mechanics*, 1983, pp. 13–25.
8. G. W. Hollingshed, 'Stress distributions in rock anchors', *Canad. Geotech. J.* **8**, 588–592 (1971).
9. O. Aydan, 'The stabilization of engineering structures by rockbolts', *Ph.D. Thesis*, Nagoya University, 1989.
10. Tao Zhen Yu and Chen Jie Xian, 'Behaviour of rock bolting as tunnelling support', in O. Stephansson (ed.), *Proc. Int. J. Symp. Rock Bolting*, Abisko, 1983, pp. 87–92.
11. B. Indranatna and P. K. Kaiser, 'Analytical model for the design of grouted rock bolts., *Int. J. numer. anal. methods geomech.*, **14**, 227–251 (1991).
12. Sun Xueyi, 'Grouted rock bolt used in undergound engineering in soft surrounding rock or in highly stressed regions', in O. Stephansson (ed.), *Proc. Int. Symp. Rock Bolting*, Abisko, 1983, pp. 345–352.
13. S. S. Peng and L. B. Guo, 'A hybrid boundary-element-finite element method of stress analysis for bolt-reinforced inhomogeneous rock', *Mining Sci. Technol.*, **7**, 1–18 (1988).
14. P. G. Fuller and R. H. T. Cox, 'Mechanics of load transfer from steel tendons to cement based grout', *Proc. 5th Aust. Conf. the Mechanics of Structures and Materials*, Melbourne, 1975, pp. 189–203.
15. J. M. Goris, 'Laboratory evaluation of Cable Bolt Supports', *92nd Annual General Meeting of the CIM*, Ottawa, 1990.
16. A. J. Hyett, W. F. Bawden and R. D. Reichert, 'The effect of rock mass confinement on the bond strength of fully grouted cable bolts', *Int. J. Rock Mech. Min. Sci. Geomech. Abstr.*, **29**, 503–524 (1992).
17. A. J. Hyett, W. F. Bawden, G. R. MacSporran and M. Moosavi, 'A constitutive law for bond failure of fully grouted cable bolts using a Modified Hoek Cell', *Int. J. of Rock Mech. Min. Sci Geomech. Abstr.*, **32**, 11–36 (1995).
18. L. Obert and W. I. Duvall, *Rock Mechanics and the Design of Structures in Rock*, Wiley, New York, 1967.
19. S. Sakurai and I. Kawashima. 'Modelling of jointed rock masses reinforced by bolts', in P. K. Kaser and D. R. McCreath (eds.) *Proc. Int. Symp. Rock Support*, Sudbury, 1992, pp. 547–550.